

QCD NLO predictions to W -pair production in association with a massive (anti)bottom-jet at the LHC

Yan Han, Wang Shao-Ming, Ma Wen-Gan, Zhang Ren-You, and Guo Lei

Department of Modern Physics, University of Science and Technology
of China (USTC), Hefei, Anhui 230026, P.R.China

Abstract

The W -pair production in association with a massive (anti)bottom jet is not only an important background to a number of interesting processes, such as the single top production associated with a W boson, but also a potential background to new physics searches. We present the calculations of the total and differential cross sections for the $W^+W^- + b(\bar{b})$ jet productions at the LHC up to the QCD next-to-leading order (NLO). Our results by adopting the QCD NLO contribution collection scheme-I show that the K factors can be 1.66 and 1.21 with the inclusive and exclusive two-jet event selection schemes respectively, when we set $m_H = 120 \text{ GeV}$, $\mu = m_W + m_b/2$ and take the constraints of $p_{T,b(\bar{b})} > 25 \text{ GeV}$, $|y_{b(\bar{b})}| < 2.5$ for $b(\bar{b})$ jet. We find that the stabilization of the theoretical prediction for the integrated cross section for the $pp \rightarrow W^+W^-b(\bar{b}) + X$ up to the QCD NLO requires a veto on a second isolated hard jet and the inclusion of the QCD NLO contribution from the $W^+W^-b\bar{b}(bb, \bar{b}\bar{b})$ production with the final two $b(\bar{b})$ quarks being merged as one jet.

PACS: 12.38.Bx, 13.85.Lg, 14.65.Ha, 14.70.Fm

I. Introduction

At the LHC, the single top associated production, $pp \rightarrow bg \rightarrow Wt + X$, offers a unique possibility of the direct measurement of the entry V_{tb} of the Cabibbo-Kobayashi-Maskawa quark-mixing matrix (CKM), allowing nontrivial tests of the properties of this matrix in the standard model (SM)[1, 2, 3]. By this channel we can also study the $W - t - b$ vertex, and test precisely the V-A structure of the charged current weak interaction of the top quark by looking at the polarization of this quark[3, 4]. Furthermore, such a production channel could be interesting in hunting for new physics beyond the SM. The new physics may manifest itself via either loop effects, or inducing non-SM weak interactions to introduce new single top production channels[5]. The produced top quark of the $pp \rightarrow bg \rightarrow Wt + X$ process subsequently decays mainly into a W boson and a bottom quark, therefore, the observed final states of the single top-quark production in association with a W boson are mostly W^+W^-b where the two W bosons can be reconstructed from their leptonic decay products. The similar analysis also applies for the $pp \rightarrow W^+W^-\bar{b} + X$ process.

Besides, the Higgs boson can be produced in association with a high p_T jet. If the SM Higgs boson is in the intermediate mass range, the $pp \rightarrow H^0 + \text{jet} \rightarrow W^+W^- + \text{jet}$ process is expected to be a discovery channel for the Higgs boson, particularly if the Higgs-boson mass is very close to the threshold for the W -pair production. B. Mellado, *et al.*, conclude in their paper[6] that the Higgs signal significance can be improved by considering also the final states which consist of the leptonic decays of the W pair, and at least one additional jet. They suggest that the Higgs boson associated with only a single jet at large rapidity is requested as a signal. They find that the backgrounds can be reduced substantially and the sensitivity of experiments can be enhanced in the search for the Higgs boson via the $W^+W^- + \text{jet}$ production channel. The QCD next-to-leading order (NLO) corrections to the process $pp \rightarrow W^+W^-j + X$ were studied in Refs.[7, 8]. In these papers the initial quark $q \neq b, \bar{b}$ was assumed, and the subprocesses with $j = b, \bar{b}$ in final states are excluded for the reason that such processes can be excluded by anti- b tagging or should be seen as continuations of W^-t or $W^+\bar{t}$ production. Since the process $pp \rightarrow W^+W^-b(\bar{b}) + X$ at the LHC is an essential background of both the single top production and the single Higgs-

boson production channels, the investigation of it can serve as a complementary work for those presented in Refs.[7, 8]. Furthermore, the process $pp \rightarrow W^+W^-b(\bar{b}) + X$ is interesting in its own right, since W -pair production processes enable a direct precise probing of the nonabelian gauge boson couplings. To sum up, improving the precision of the predictions for the $W^+W^-b(\bar{b})$ production is necessary, since $W^+W^- + b(\bar{b})$ -jet production delivers not only the background to a number of interesting processes, but also a potential background to new physics searches.

In this work, we perform the calculations for the QCD NLO corrections to the $pp \rightarrow W^+W^-b(\bar{b}) + X$ process. Within this work, the mass of bottom quark is retained in all the partonic processes. The paper is organized as follows. We present the details of the calculation strategies in Sec. II. The numerical results and discussions are given in Sec. III, and finally a short summary is given.

II. Strategies in calculation

We neglect the quark mixing between the two light and the third massive generations (i.e., $V_{ub} = V_{cb} = V_{td} = V_{ts} \sim 0$), and take the u, d, c, s quark being massless ($m_u = m_d = m_c = m_s = 0$) and the bottom-quark being massive. We use the five-flavor scheme (5FS) in the leading-order (LO) and QCD NLO calculations. The difference between adopting the five-flavor scheme and four-flavor scheme is the ordering of the perturbative series for the production cross section. In the four-flavor scheme the perturbative series is ordered strictly by powers of the strong coupling α_s , while in the 5FS the introduction of the b quark parton distribution function (PDF) allows to resum terms of the form $\alpha_s^n \ln(\mu^2/m_b^2)^m$ at all orders in α_s . The calculations are carried out in the 't Hooft-Feynman gauge. The FEYNARTS 3.4 package[9] is adopted to generate Feynman diagrams and convert them to the corresponding amplitudes. FORMCALC 5.4 programs[10] are implemented to simplify the amplitudes. As we know the cross section for the $gb \rightarrow W^+W^-b$ partonic process in the SM should be the same as that for its charge conjugate subprocess $g\bar{b} \rightarrow W^+W^-\bar{b}$, and the luminosity of the bottom-quark in proton is the same as that of the antibottom quark. Therefore, the production rates for both the W^+W^-b and the $W^+W^-\bar{b}$ productions at the LHC are identical. In the following sections we present only the analytical calculations of the related partonic process $gb \rightarrow W^+W^-b$ and the parent

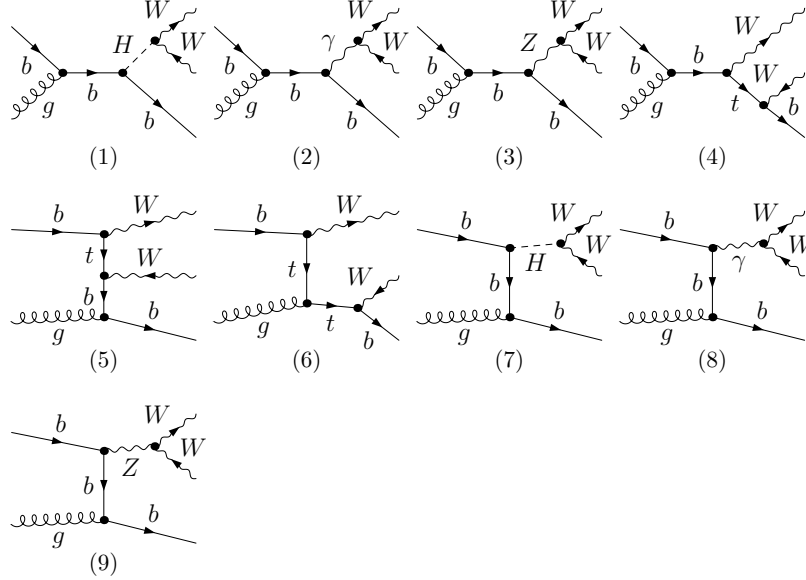


Figure 1: The LO Feynman diagrams for the partonic process $gb \rightarrow W^+W^-b$, where the internal top-quark in Figs.1(4,6) and the Higgs boson in Figs.1(1,7) may be on mass shell.

process $pp \rightarrow W^+W^-b + X$ unless otherwise indicated.

II.1 Leading order cross sections

We denote the concerned partonic process as $g(p_1) + b(p_2) \rightarrow W^+(p_3) + W^-(p_4) + b(p_5)$. There are nine leading order (LO) Feynman diagrams for this partonic process shown in Fig.1. There Figs.1(1-4) and Figs.1(5-9) are the s-channel and t-channel diagrams for the partonic process, respectively. The LO cross section for the partonic process $gb \rightarrow W^+W^-b$ is obtained by using the following formula:

$$\hat{\sigma}_{LO}(\hat{s}, gb \rightarrow W^+W^-b) = \frac{(2\pi)^4}{4|\vec{p}_1|\sqrt{\hat{s}}} \int \overline{\sum} |\mathcal{M}_{LO}|^2 d\Phi_3, \quad (2.1)$$

where $d\Phi_3$ is the three-body phase-space element, and \vec{p}_1 is the momentum of the initial gluon in the center-of-mass system. The integration is performed over the three-body phase space of the final particles W^+W^-b . The summation is taken over the spins and colors of the initial and final states, and the bar over the summation indicates averaging over the intrinsic degrees of freedom of initial partons.

In the LO calculations, the internal top quark and Higgs boson are potentially resonant. We introduce the complex mass scheme(CMS)[11] to deal with the internal resonant top quark

and Higgs boson. In the CMS the complex masses of the unstable top quark and Higgs boson should be taken everywhere in both tree-level and one-loop level calculations. Then the gauge invariance is conserved and the singularity poles of propagators for real p^2 are avoided. The relevant complex masses are defined as $\mu_t^2 = m_t^2 - im_t\Gamma_t$, $\mu_H^2 = m_H^2 - im_H\Gamma_H$, where m_t and m_H are the conventional real masses, Γ_t and Γ_H represent the corresponding total widths of the top quark and Higgs boson, and the poles of propagators are located at μ_t^2 and μ_H^2 on the complex p^2 plane, respectively. Since the unstable particles are involved in the loops for the $\mathcal{O}(\alpha_s)$ QCD corrections, we shall meet the calculations of N point integrals with complex masses.

The LO total cross section for $pp \rightarrow W^+W^-b + X$ can be expressed as

$$\sigma_{LO}(pp \rightarrow W^+W^-b + X) = \int dx_A dx_B \left[G_{g/A}(x_A, \mu_f) G_{b/B}(x_B, \mu_f) \hat{\sigma}_{LO}(gb \rightarrow W^+W^-b, x_A x_B s, \mu_f, \mu_r) + (A \leftrightarrow B) \right]. \quad (2.2)$$

There $G_{i/P}$ ($i = g, b$, $P = A, B$) represent the PDFs of parton i in proton P , μ_f and μ_r are the factorization and renormalization scales separately, and x_A and x_B describe the momentum fractions of parton (gluon or bottom-quark) in protons A and B respectively.

II.2 QCD NLO corrections

II.2.1 General description

Our jet recombination procedure is based on the jet algorithm in Ref.[12]. We consider the jet events with up to two protojets involved in the final states. The candidate jet events are applied by the jet recombination procedure with the following criteria: If the two protojets i and j satisfy $\sqrt{\Delta\eta^2 + \Delta\phi^2} < R \equiv 0.7$ (where $\Delta\eta$ and $\Delta\phi$ are the differences of pseudorapidity and the azimuthal angle between the two protojets), they are merged as one jet and this jet event is called a one-jet event, whose four-momentum is defined as $p_{ij,\mu} = p_{i,\mu} + p_{j,\mu}$. The transverse momentum and rapidity of the merged jet are calculated from its four-momentum by using the formulas $p_{ij,T} = \sqrt{p_{ij,x}^2 + p_{ij,y}^2}$ and $y_{ij} = \frac{1}{2} \ln \left(\frac{E_{ij} + p_{ij,L}}{E_{ij} - p_{ij,L}} \right)$.

The QCD NLO correction to the $pp \rightarrow W^+W^-b + X$ process includes the following components:

- (i) The QCD one-loop virtual corrections to the partonic process $gb \rightarrow W^+W^-b$.
- (ii) The contribution of the real gluon emission partonic process $gb \rightarrow W^+W^-bg$.
- (iii) The contribution of the real light-(anti)quark emission partonic process $qb \rightarrow W^+W^-bq$, where q denotes any of the light-(anti)quarks $u, d, c, s, \bar{u}, \bar{d}, \bar{c}, \bar{s}$.
- (iv) The corresponding contributions of the PDF counterterms.
- (v) The additional contributions of the PDFs for subtracting the quasicollinear mass singularity from massive bottom quark.

In order to make a comparison, we use two schemes for the collection of the finite contributions at $\mathcal{O}(\alpha_s^2\alpha_{ew}^2)$. In the QCD NLO contribution collection scheme-I, we collect only the five components mentioned above for the QCD NLO corrections. In the QCD NLO contribution collection scheme-II, in addition to the contributions involved in the collection scheme-I, the QCD NLO corrections to the $pp \rightarrow W^+W^-b + X$ process include the following three additional contributions:

- (i) The LO contribution of the (anti)bottom-quark radiative processes $q\bar{q}(gg) \rightarrow W^+W^-b\bar{b}$ ($q = u, d, c, s, b$) in the "merged one-jet phase space" (One half contribution belongs to the QCD NLO correction of the $pp \rightarrow W^+W^-b + X$ process, another half is to the correction of the $pp \rightarrow W^+W^-b + X$ process).
- (ii) The LO contributions of the $pp \rightarrow bb \rightarrow W^+W^-bb$ and $pp \rightarrow \bar{b}\bar{b} \rightarrow W^+W^-\bar{b}\bar{b}$ processes in the "merged one-jet phase space" (The contribution from the former process belongs to the $pp \rightarrow W^+W^-b + X$ process, the latter part belongs to the $pp \rightarrow W^+W^-b + X$ process).
- (iii) The additional contributions of the PDFs and fragmentation functions (FFs) for subtracting the quasicollinear mass singularities in the $pp \rightarrow W^+W^-b\bar{b}(bb, \bar{b}\bar{b})$ processes.

The so-called "merged one-jet phase space" is defined where the two final $b(\bar{b})$ jets are merged as one jet in the tagging region of the detector, i.e., $\sqrt{\Delta\eta^2 + \Delta\phi^2} < 0.7$, and the merged jet

passes the constraints of $p_{T,j} > 25 \text{ GeV}$ and $|y_j| < 2.5$. That is to say the two (anti)bottom quarks cannot form two isolated hard jets, and therefore we call the event a one-jet event. We notice that all the contributions involved in the QCD NLO contribution collection scheme-II are at $\mathcal{O}(\alpha_s^2 \alpha_{ew}^2)$.

The dimensional regularization method in $D = 4 - 2\epsilon$ dimensions is used to isolate the UV and IR singularities. We split each collinear counterterm of the PDF, $\delta G_{i/P}(x, \mu_f)$ ($P = \text{proton}$, $i = g, u, \bar{u}, d, \bar{d}, c, \bar{c}, s, \bar{s}$), into two parts: the collinear gluon emission part $\delta G_{i/P}^{(gluon)}(x, \mu_f)$ and the collinear light-quark emission part $\delta G_{i/P}^{(quark)}(x, \mu_f)$. The analytical expressions are presented as follows.

$$\delta G_{q(g)/P}(x, \mu_f) = \delta G_{q(g)/P}^{(gluon)}(x, \mu_f) + \delta G_{q(g)/P}^{(quark)}(x, \mu_f), \quad (q = u, \bar{u}, d, \bar{d}, c, \bar{c}, s, \bar{s}), \quad (2.3)$$

where

$$\begin{aligned} \delta G_{q(g)/P}^{(gluon)}(x, \mu_f) &= \frac{1}{\epsilon} \left[\frac{\alpha_s}{2\pi} \frac{\Gamma(1-\epsilon)}{\Gamma(1-2\epsilon)} \left(\frac{4\pi\mu_r^2}{\mu_f^2} \right)^\epsilon \right] \int_x^1 \frac{dz}{z} P_{qq(gg)}(z) G_{q(g)/P}(x/z, \mu_f), \\ \delta G_{q/P}^{(quark)}(x, \mu_f) &= \frac{1}{\epsilon} \left[\frac{\alpha_s}{2\pi} \frac{\Gamma(1-\epsilon)}{\Gamma(1-2\epsilon)} \left(\frac{4\pi\mu_r^2}{\mu_f^2} \right)^\epsilon \right] \int_x^1 \frac{dz}{z} P_{qg}(z) G_{g/P}(x/z, \mu_f), \\ \delta G_{g/P}^{(quark)}(x, \mu_f) &= \frac{1}{\epsilon} \left[\frac{\alpha_s}{2\pi} \frac{\Gamma(1-\epsilon)}{\Gamma(1-2\epsilon)} \left(\frac{4\pi\mu_r^2}{\mu_f^2} \right)^\epsilon \right] \sum_{q=u, \bar{u}}^{d, \bar{d}, c, \bar{c}, s, \bar{s}} \int_x^1 \frac{dz}{z} P_{gq}(z) G_{q/P}(x/z, \mu_f), \end{aligned} \quad (2.4)$$

and the explicit expressions for the splitting functions $P_{ij}(z)$, ($ij = qq, qg, gq, gg$) can be found in Ref.[13].

II.2.2 Virtual and real emission corrections to $gb \rightarrow W^+ W^- b$

The amplitude at the one-loop level for the partonic process $gb \rightarrow W^+ W^- b$ in the SM contains the contributions of the self-energy, vertex, box, pentagon and counterterm graphs. In Fig.2 the four pentagon Feynman diagrams are shown as representatives.

In order to remove the UV divergences in virtual corrections, we need to renormalize the strong coupling constant, the masses and wave functions of the relevant colored particles. In our calculations we introduce the following renormalization constants:

$$\begin{aligned} \psi_{b(t)}^{0,L,R} &= \left(1 + \frac{1}{2} \delta Z_{b(t)}^{L,R} \right) \psi_{b(t)}^{L,R}, \quad m_b^0 = m_b + \delta m_b, \\ \mu_t^0 &= \mu_t + \delta \mu_t, \quad G_\mu^0 = (1 + \frac{1}{2} \delta Z_g) G_\mu, \quad g_s^0 = g_s + \delta g_s, \end{aligned} \quad (2.5)$$

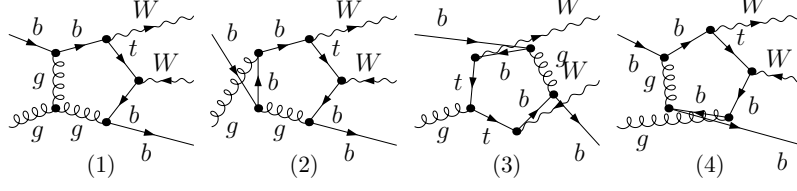


Figure 2: The pentagon Fynman diagrams for the partonic process $gb \rightarrow W^+W^-b$.

where g_s denotes the strong coupling constant, m_b and μ_t are bottom-quark mass and top-quark complex mass, respectively, and $\psi_b^{L,R}$, $\psi_t^{L,R}$, and G_μ denote the fields of bottom quark, top quark and gluon, separately. The masses and wave functions of the colored fields are renormalized in the on-shell scheme, and the relevant counterterms are expressed as

$$\begin{aligned}
\delta Z_b^{L,R} &= -\frac{\alpha_s(\mu_r)}{3\pi} \left[\Delta_{UV} + 2\Delta_{IR} + 4 + 3 \ln \left(\frac{\mu_r^2}{m_b^2} \right) \right], \\
\delta Z_t^{L,R} &= -\frac{\alpha_s(\mu_r)}{3\pi} \left[\Delta_{UV} + 2\Delta_{IR} + 4 + 3 \ln \left(\frac{\mu_r^2}{\mu_t^2} \right) \right], \\
\frac{\delta m_b}{m_b} &= -\frac{\alpha_s(\mu_r)}{3\pi} \left\{ 3 \left[\Delta_{UV} + \ln \left(\frac{\mu_r^2}{m_b^2} \right) \right] + 4 \right\}, \\
\frac{\delta \mu_t}{\mu_t} &= -\frac{\alpha_s(\mu_r)}{3\pi} \left\{ 3 \left[\Delta_{UV} + \ln \left(\frac{\mu_r^2}{\mu_t^2} \right) \right] + 4 \right\}, \\
\delta Z_g &= -\frac{\alpha_s(\mu_r)}{2\pi} \left\{ -\frac{1}{2} \Delta_{UV} + \frac{7}{6} \Delta_{IR} + \frac{1}{3} \left[\ln \left(\frac{\mu_r^2}{m_b^2} \right) + \ln \left(\frac{\mu_r^2}{\mu_t^2} \right) \right] \right\}, \quad (2.6)
\end{aligned}$$

where $\Delta_{UV} = 1/\epsilon_{UV} - \gamma_E + \ln(4\pi)$ and $\Delta_{IR} = 1/\epsilon_{IR} - \gamma_E + \ln(4\pi)$.

For the renormalization of the strong coupling constant g_s , we adopt the \overline{MS} scheme at the renormalization scale μ_r , except that the divergences associated with the massive top- and bottom-quark loops are subtracted at zero momentum[14]. Then the counterterm of the strong coupling constant g_s can be obtained as

$$\frac{\delta g_s}{g_s} = -\frac{\alpha_s(\mu_r)}{4\pi} \left[\frac{\beta_0}{2} \Delta_{UV} + \frac{1}{3} \ln \frac{m_b^2}{\mu_r^2} + \frac{1}{3} \ln \frac{\mu_t^2}{\mu_r^2} \right], \quad (2.7)$$

where $\beta_0 = \frac{11}{3}N - \frac{2}{3}N_f - \frac{4}{3}$, and the numbers of colors and active flavors are taken as $N = 3$ and $N_f = 4$ respectively. As shown in Eqs.(2.6) and (2.7), the renormalizaion constants δZ_g , $\delta Z_b^{L,R}$, δm_b and $\delta g_s/g_s$ contain the terms of $\alpha_s \ln \left(\frac{\mu_r^2}{m_b^2} \right)$, which is divergent when $m_b \rightarrow 0$. Therefore, the amplitude of the counterterms for the subprocess $gb \rightarrow W^+W^-b$ also contains the quasi-collinear mass-singular term. By adding the virtual and real corrections to the contributions of

counterterms, the $\mathcal{O}(\alpha_s^2 \alpha_{ew}^2)$ NLO QCD corrected partonic cross section still involves the quasicollinear mass-singular term, which could violate the convergence of the perturbative series. But this quasicollinear mass-singular term can be canceled exactly by the additional contributions of the PDFs and the FFs for subtracting the quasicollinear mass singularity due to the massive bottom quark, as explained in the following subsection.

Because we use the CMS to deal with the possible top-quark and Higgs-boson resonances, the normal one-loop integrals must be continued onto the complex plane. The formulas for calculating the IR-divergent integrals with complex internal masses in the dimensional regularization scheme are obtained by analytically continuing the expressions in Ref.[15] onto the complex plane. The numerical evaluations of IR-safe N point ($n = 1, 2, 3, 4, 5$) integrals with complex masses, are implemented by using the expressions analytically continued onto the complex plane from those presented in Refs.[16, 17, 18]. In this way, we created our in-house subroutines to isolate analytically the IR singularities in integrals and calculate numerically one-loop integrals with complex masses based on the LOOPTOOLS-2.4 package[10][19].

The corrections due to the real gluon and (anti)light-quark emission partonic processes, $b(p_1) g[q, \bar{q}](p_2) \rightarrow W^+(p_3) W^-(p_4) b(p_5) g[q, \bar{q}](p_6)$ ($q = u, d, c, s$), are dealt with by using the two cutoff phase-space slicing method[13]. The soft IR singularity of the real gluon emission subprocess can be isolated by introducing an arbitrary soft cutoff δ_s , to separate the $2 \rightarrow 4$ phase space into two regions, $E_6 \leq \delta_s \sqrt{\hat{s}}/2$ (soft gluon region) and $E_6 > \delta_s \sqrt{\hat{s}}/2$ (hard gluon region). The cutoff δ_c decomposes the real hard gluon/(anti)light-quark emission phase-space region into hard collinear (HC) region, $\hat{s}_{26} < \delta_c \hat{s}$ (where $\hat{s}_{ij} = (p_i + p_j)^2$), and noncollinear (\overline{HC}) region, $\hat{s}_{26} > \delta_c \hat{s}$, in order to isolate the collinear singularity from the IR-safe region. The integration over the \overline{HC} region of phase space can be performed in the four-dimensions by using the program based on the VEGAS, a Monte Carlo integrator[20]. Then the cross section for the real emission processes can be written as

$$\Delta\sigma_R = \Delta\sigma_S + \Delta\sigma_H = \Delta\sigma_S + \Delta\sigma_{HC} + \Delta\sigma_{\overline{HC}}. \quad (2.8)$$

The UV singularities in the virtual corrections are canceled by the contributions of all the related counterterms. Soft and collinear IR singularities are also involved in virtual corrections.

After combining the contributions of the real gluon/light-quark emission processes and the PDF counterterms $\delta G_{q(g)/P}$ with the virtual contributions together, these IR singularities are exactly vanished. These cancelations have been verified numerically in our numerical calculations.

II..2.3 Subtraction of quasicollinear mass singularity

Since the bottom-quark mass is retained within the whole calculation, the PDFs of (anti)bottom quark and gluon (up to the α_s order) contain the large logarithm terms of $\left(\alpha_s \ln \frac{\mu_f^2}{m_b^2}\right)$. The large logarithm terms in the $G_{b(\bar{b})/P}(x, \mu_f)$ and $G_{g/P}(x, \mu_f)$ PDFs arise from the (anti)bottom-quark emission off the (anti)bottom quark or gluon and gluon emission off the (anti)bottom quark, respectively. They are just the QCD NLO counterterms of $G_{b(\bar{b})/P}(x, \mu_f)$ and $G_{g/P}(x, \mu_f)$ which are finite with a nonzero bottom-quark mass. The isolation of these quasicollinear mass-singular terms are similar to that in the conventional massless parton model approach.

Analogous to the PDFs of light quarks ($q = u, \bar{u}, d, \bar{d}, c, \bar{c}, s, \bar{s}$) in Eq.(2.3), the QCD NLO counterterm of $G_{b(\bar{b})/P}(x, \mu_f)$ can be split into the gluon emission part and the $\bar{b}(b)$ emission part.

$$\delta G_{b(\bar{b})/P}(x, \mu_f) = \delta G_{b(\bar{b})/P}^{(gluon)}(x, \mu_f) + \delta G_{b(\bar{b})/P}^{(\bar{b}(b))}(x, \mu_f). \quad (2.9)$$

The explicit expressions for these two components can be expressed as[21, 22]

$$\begin{aligned} \delta G_{b(\bar{b})/P}^{(gluon)}(x, \mu_f) &= -\frac{\alpha_s}{2\pi} \int_x^1 \frac{dz}{z} \left[P_{bb(\bar{b}\bar{b})}(z) \left(\ln \frac{\mu_f^2}{m_b^2} - 2 \ln(1-z) - 1 \right) \right]_+ G_{b(\bar{b})/P}(x/z, \mu_f) \\ \delta G_{b(\bar{b})/P}^{(\bar{b}(b))}(x, \mu_f) &= -\frac{\alpha_s}{2\pi} \int_x^1 \frac{dz}{z} P_{bg(\bar{b}g)}(z) \left(\ln \frac{\mu_f^2}{m_b^2} \right) G_{g/P}(x/z, \mu_f), \end{aligned} \quad (2.10)$$

where the $[\dots]_+$ prescription is defined by

$$\int_x^1 dz [f(z)]_+ g(z) = \int_x^1 dz f(z) g(z) - \int_0^1 dz f(z) g(1) \quad . \quad (2.11)$$

Obviously these two counterterms are proportional to $\left(\alpha_s \ln \frac{\mu_f^2}{m_b^2}\right)$ and finite with nonzero bottom-quark mass.

The QCD NLO counterterm of $G_{g/P}(x, \mu_f)$ is also divided into two components. Among them one is the divergent, whose analytical expression is proportional to $\frac{1}{\epsilon} \left[\frac{\alpha_s}{2\pi} \frac{\Gamma(1-\epsilon)}{\Gamma(1-2\epsilon)} \left(\frac{4\pi\mu_f^2}{\mu_f^2} \right)^\epsilon \right]$,

and has been given in Eqs.(2.3) and (2.4). Another component is the additional part, $\delta G_{g/P}^{(add)}(x, \mu_f)$, which is proportional to $\left(\alpha_s \ln \frac{\mu_f^2}{m_b^2}\right)$, i.e.,

$$\begin{aligned}\delta G_{g/P}^{(add)}(x, \mu_f) &= \delta G_{g/P}^{(b)}(x, \mu_f) + \delta G_{g/P}^{(\bar{b})}(x, \mu_f) \\ &= -\frac{\alpha_s}{2\pi} \int_x^1 \frac{dz}{z} P_{gb}(z) \left(\ln \frac{\mu_f^2}{m_b^2} \right) G_{b/P}(x/z, \mu_f) \\ &\quad -\frac{\alpha_s}{2\pi} \int_x^1 \frac{dz}{z} P_{g\bar{b}}(z) \left(\ln \frac{\mu_f^2}{m_b^2} \right) G_{\bar{b}/P}(x/z, \mu_f).\end{aligned}\quad (2.12)$$

In order to include the contributions of these quasicollinear mass-singular counterterms of the PDFs in the total NLO cross section, we replace the PDFs in the expressions for $\sigma_{LO}(pp \rightarrow W^+W^-b + X)$ and $\sigma_{LO}(pp \rightarrow W^+W^-\bar{b} + X)$ (see Eq.(2.2) for $\sigma_{LO}(pp \rightarrow W^+W^-b + X)$ and similar one for $\sigma_{LO}(pp \rightarrow W^+W^-\bar{b} + X)$) as

$$\begin{aligned}G_{b(\bar{b})/P}(x, \mu_f) &\longrightarrow G_{b(\bar{b})/P}(x, \mu_f) + \delta G_{b(\bar{b})/P}^{(gluon)}(x, \mu_f) + \delta G_{b(\bar{b})/P}^{(\bar{b}(b))}(x, \mu_f), \\ G_{g/P}(x, \mu_f) &\longrightarrow G_{g/P}(x, \mu_f) + \delta G_{g/P}^{(gluon)}(x, \mu_f) + \delta G_{g/P}^{(quark)}(x, \mu_f) + \delta G_{g/P}^{(add)}(x, \mu_f).\end{aligned}\quad (2.13)$$

Then we obtain the following five additional contributions of the PDFs:

$$\begin{aligned}(i) \quad &\sigma_{PDF}(W^+W^-bg) \\ &= \int dx_A dx_B \left[G_{g/A}(x_A, \mu_f) \delta G_{b/B}^{(gluon)}(x_B, \mu_f) \hat{\sigma}_{LO}(gb \rightarrow W^+W^-b) + (A \leftrightarrow B) \right], \\ (ii) \quad &\sigma_{PDF}(W^+W^-\bar{b}g) \\ &= \int dx_A dx_B \left[G_{g/A}(x_A, \mu_f) \delta G_{\bar{b}/B}^{(gluon)}(x_B, \mu_f) \hat{\sigma}_{LO}(g\bar{b} \rightarrow W^+W^-\bar{b}) + (A \leftrightarrow B) \right], \\ (iii) \quad &\sigma_{PDF}(W^+W^-bb) \\ &= \int dx_A dx_B \left[G_{b/A}(x_A, \mu_f) \delta G_{g/B}^{(b)}(x_B, \mu_f) \hat{\sigma}_{LO}(gb \rightarrow W^+W^-b) + (A \leftrightarrow B) \right], \\ (iv) \quad &\sigma_{PDF}(W^+W^-\bar{b}\bar{b}) \\ &= \int dx_A dx_B \left[G_{\bar{b}/A}(x_A, \mu_f) \delta G_{g/B}^{(\bar{b})}(x_B, \mu_f) \hat{\sigma}_{LO}(g\bar{b} \rightarrow W^+W^-\bar{b}) + (A \leftrightarrow B) \right], \\ (v) \quad &\sigma_{PDF}(W^+W^-b\bar{b}) \\ &= \sigma_{PDF}^{(gg)}(W^+W^-b\bar{b}) + \sigma_{PDF}^{(b\bar{b})}(W^+W^-b\bar{b}) \\ &= \int dx_A dx_B \left[G_{g/A}(x_A, \mu_f) \delta G_{b/B}^{(\bar{b})}(x_B, \mu_f) \hat{\sigma}_{LO}(gb \rightarrow W^+W^-b) \right. \\ &\quad \left. + G_{g/A}(x_A, \mu_f) \delta G_{\bar{b}/B}^{(b)}(x_B, \mu_f) \hat{\sigma}_{LO}(g\bar{b} \rightarrow W^+W^-\bar{b}) + (A \leftrightarrow B) \right],\end{aligned}$$

$$\begin{aligned}
& + G_{g/A}(x_A, \mu_f) \delta G_{\bar{b}/B}^{(b)}(x_B, \mu_f) \hat{\sigma}_{LO}(g\bar{b} \rightarrow W^+ W^- \bar{b}) + (A \leftrightarrow B) \Big] \\
& + \int dx_A dx_B \Big[G_{b/A}(x_A, \mu_f) \delta G_{g/B}^{(\bar{b})}(x_B, \mu_f) \hat{\sigma}_{LO}(gb \rightarrow W^+ W^- b) \\
& + G_{\bar{b}/A}(x_A, \mu_f) \delta G_{g/B}^{(b)}(x_B, \mu_f) \hat{\sigma}_{LO}(g\bar{b} \rightarrow W^+ W^- \bar{b}) + (A \leftrightarrow B) \Big]. \quad (2.14)
\end{aligned}$$

From the above discussion we can see that the large logarithm in the cross section $\sigma(pp \rightarrow gg \rightarrow W^+ W^- b\bar{b} + X)$ is canceled exactly by that in the additional PDF contribution $\sigma_{PDF}^{(gg)}(W^+ W^- b\bar{b})$ shown in Eq.(2.14). To cancel the quasicollinear mass singularity of the $pp \rightarrow b\bar{b} \rightarrow W^+ W^- b\bar{b} + X$ process, both the additional contributions of the PDFs and the FFs should be included, since the quasicollinear mass singularity arises not only from the (anti)bottom-quark emission off the initial (anti)bottom quark, but also the gluon splitting to the $b\bar{b}$ pair in the final states. For the $pp \rightarrow q\bar{q} \rightarrow W^+ W^- b\bar{b} + X$ ($q = u, d, c, s$) processes there also exists a large logarithm corresponding to the final gluon splitting to the $b\bar{b}$ pair, which can be absorbed by the additional FF contribution. The FF additional contribution to the cross section can be expressed as[22]

$$\begin{aligned}
& \sigma_{FF}^{(q\bar{q})}(W^+ W^- b\bar{b}) \\
& = - \int dx_A dx_B dz \Big[G_{q/A}(x_A, \mu_f) G_{\bar{q}/B}(x_B, \mu_f) \hat{\sigma}_{LO}(q\bar{q} \rightarrow W^+ W^- g) \frac{\alpha_s}{2\pi} P_{bg}(z) \left(\ln \frac{\mu_f^2}{m_b^2} \right) \right. \\
& \quad \left. + (A \leftrightarrow B) \Big], \quad (q = u, d, c, s, b). \quad (2.15)
\end{aligned}$$

II.3 Cancellation of quasicollinear mass-singularity

The quasicollinear mass singularity of the real gluon emission process $pp \rightarrow gb \rightarrow W^+ W^- bg + X$ arises from the gluon emission off either the initial or the final bottom quark. The large logarithm term corresponding to the gluon emission off the initial bottom quark is canceled by that of $\sigma_{PDF}(W^+ W^- bg)$, while the large logarithm term corresponding to the gluon emission off the final bottom quark is canceled by that of the virtual corrections to the $pp \rightarrow W^+ W^- b + X$ process exactly. For the real light-quark emission processes $pp \rightarrow qb \rightarrow W^+ W^- bq + X$ ($q = u, \bar{u}, d, \bar{d}, c, \bar{c}, s, \bar{s}$), the final bottom quark is noncollinear to the initial bottom quark since a bottom jet should be detected in the final states. Therefore, the real light-quark emission processes $pp \rightarrow qb \rightarrow W^+ W^- bq + X$ ($q = u, \bar{u}, d, \bar{d}, c, \bar{c}, s, \bar{s}$) do not contain quasicollinear mass singularity.

After the cancelation of quasicollinear mass singularity explained above, we get the total QCD NLO correction to the $pp \rightarrow W^+W^-b + X$ process by adopting the QCD NLO contribution collection scheme-I (see next section), which is free of the contribution from the large logarithm term $\left(\alpha_s \ln \frac{\mu_f^2}{m_b^2}\right)$, expressed as

$$\begin{aligned} & \Delta\sigma_{NLO}(pp \rightarrow W^+W^-b + X) \\ &= \sum_{q=u,d,c,s}^{\bar{u},\bar{d},\bar{c},\bar{s}} \Delta\sigma_R(pp \rightarrow qb \rightarrow W^+W^-bq + X) + [\Delta\sigma_V(pp \rightarrow gb \rightarrow W^+W^-b + X) \\ &+ \Delta\sigma_R(pp \rightarrow gb \rightarrow W^+W^-bg + X) + \sigma_{PDF}(W^+W^-bg)] , \end{aligned} \quad (2.16)$$

We find that $\Delta\sigma_{NLO}(pp \rightarrow W^+W^-b + X)$ is convergent when $m_b \rightarrow 0$. Analogously, the total QCD NLO correction to the $pp \rightarrow W^+W^-\bar{b} + X$ process, which is the summation of the virtual, real corrections and $\sigma_{PDF}(W^+W^-\bar{b}g)$, is also finite when $m_b \rightarrow 0$.

There are 28 Feynman diagrams for the $pp \rightarrow bb \rightarrow W^+W^-bb + X$ process at the $\mathcal{O}(\alpha_s^2\alpha_{ew}^2)$. We can find that one (and only one) of the two final bottom quarks is emitted off the initial bottom quarks for each of these Feynman diagrams, therefore, the cross section for the $pp \rightarrow bb \rightarrow W^+W^-bb + X$ process contains the large logarithm term of $\alpha_s \ln \left(\frac{\mu_f^2}{m_b^2}\right)$. This quasicollinear mass singular term is canceled exactly by that of $\sigma_{PDF}(W^+W^-bb)$. Similarly, the large logarithm terms in $\sigma(pp \rightarrow \bar{b}\bar{b} \rightarrow W^+W^-\bar{b}\bar{b} + X)$ and $\sigma_{PDF}(W^+W^-\bar{b}\bar{b})$ are canceled by each other. Then the total cross sections for the $pp \rightarrow W^+W^-bb + X$ and $pp \rightarrow W^+W^-\bar{b}\bar{b} + X$ processes defined as

$$\begin{aligned} \sigma_{tot}(pp \rightarrow W^+W^-bb + X) &= \sigma(pp \rightarrow bb \rightarrow W^+W^-bb + X) + \sigma_{PDF}(W^+W^-bb) \\ \sigma_{tot}(pp \rightarrow W^+W^-\bar{b}\bar{b} + X) &= \sigma(pp \rightarrow \bar{b}\bar{b} \rightarrow W^+W^-\bar{b}\bar{b} + X) + \sigma_{PDF}(W^+W^-\bar{b}\bar{b}), \end{aligned} \quad (2.17)$$

are convergent when $m_b \rightarrow 0$.

The quasicollinear mass singularity sources in the $pp \rightarrow W^+W^-\bar{b}\bar{b} + X$ process are listed as follows:

- (i) $pp \rightarrow q\bar{q} \rightarrow W^+W^-\bar{b}\bar{b} + X$ ($q = u, d, c, s$): the internal gluon splitting into $b\bar{b}$ -pair.
- (ii) $pp \rightarrow gg \rightarrow W^+W^-\bar{b}\bar{b} + X$: the (anti)bottom quark emitting off the initial gluon.

(iii) $pp \rightarrow b\bar{b} \rightarrow W^+W^-b\bar{b} + X$: the (anti)bottom-quark emitting off the initial (anti)bottom quark and the internal gluon splitting into $b\bar{b}$ pair.

The LO total cross section for the $pp \rightarrow W^+W^-b\bar{b} + X$ process defined as

$$\begin{aligned} \sigma_{tot}(pp \rightarrow W^+W^-b\bar{b} + X) = & \sum_{q=u,d,c,s} \left[\sigma(pp \rightarrow q\bar{q} \rightarrow W^+W^-b\bar{b} + X) + \sigma_{FF}^{(q\bar{q})}(W^+W^-b\bar{b}) \right] \\ & + \left[\sigma(pp \rightarrow b\bar{b} \rightarrow W^+W^-b\bar{b} + X) + \sigma_{PDF}^{(b\bar{b})}(W^+W^-b\bar{b}) + \sigma_{FF}^{(b\bar{b})}(W^+W^-b\bar{b}) \right] \\ & + \left[\sigma(pp \rightarrow gg \rightarrow W^+W^-b\bar{b} + X) + \sigma_{PDF}^{(gg)}(W^+W^-b\bar{b}) \right], \end{aligned} \quad (2.18)$$

which is finite when $m_b \rightarrow 0$ and would be involved in the QCD NLO corrections to the $pp \rightarrow W^+W^-b + X$ and $pp \rightarrow W^+W^-\bar{b} + X$ processes.

III. Numerical results and discussions

III.1 Input parameters

In this work we take one-loop and two-loop running α_s in the LO and NLO calculations, respectively[23]. For simplicity we set the factorization scale and the renormalization scale being equal (i.e., $\mu = \mu_f = \mu_r$) and take $\mu = \mu_0 = m_b/2 + m_W$ in default unless otherwise stated. Throughout this paper, we take $\alpha_{ew}(m_Z^2)^{-1}|_{\overline{MS}} = 127.925$, $m_W = 80.398 \text{ GeV}$, $m_Z = 91.1876 \text{ GeV}$, $\sin^2 \theta_w = 1 - \left(\frac{m_W}{m_Z}\right)^2 = 0.222646$, and set quark masses as $m_u = m_d = m_c = m_s = 0$, $m_b = 4.2 \text{ GeV}$ and $m_t = 171.2 \text{ GeV}$ [23]. The colliding energy in the proton-proton center-of-mass system is taken as $\sqrt{s} = 14 \text{ TeV}$ for the LHC. The CKM matrix elements are set as

$$V_{CKM} = \begin{pmatrix} V_{ud} & V_{us} & V_{ub} \\ V_{cd} & V_{cs} & V_{cb} \\ V_{td} & V_{ts} & V_{tb} \end{pmatrix} = \begin{pmatrix} 0.97418 & 0.22577 & 0 \\ -0.22577 & 0.97418 & 0 \\ 0 & 0 & 1 \end{pmatrix}. \quad (3.1)$$

We adopt the CTEQ6L1 and CTEQ6M PDFs in the LO and NLO calculations, respectively. The QCD parameter $\Lambda_4^{LO} = 215 \text{ MeV}$ for the CTEQ6L1 at the LO, and $\Lambda_4^{\overline{MS}} = 326 \text{ MeV}$ for the CTEQ6M at the NLO[24].

Since we take $V_{tb} \sim 1$, the decay of the top quark is dominated by the $t \rightarrow W^+b$ decay mode, and the total decay width of the top quark is approximately equal to the decay width of

$t \rightarrow W^+b$. Neglecting the terms of order m_b^2/m_t^2 , α_s^2 and $(\alpha_s/\pi)m_W^2/m_t^2$, the width predicted in the SM is [25]

$$\Gamma_t = \frac{\alpha_{ew}m_t^3}{16m_W^2s_W^2} \left(1 - \frac{m_W^2}{m_t^2}\right)^2 \left(1 + \frac{2m_W^2}{m_t^2}\right) \left[1 - \frac{2\alpha_s}{3\pi} \left(\frac{2\pi^2}{3} - \frac{5}{2}\right)\right]. \quad (3.2)$$

By taking $\alpha_{ew} = \alpha_{ew}(m_Z^2)|_{\overline{MS}} = 1/127.925$ and $\alpha_s(m_t^2) = 0.1024$, we obtain $\Gamma_t = 1.3692 \text{ GeV}$. The reasonable physical decay width of the Higgs-boson is obtained by employing the program Hdecay[26], where the partial decay width $\Gamma(H^0 \rightarrow q\bar{q})$ is calculated up to the $\mathcal{O}(\alpha_s^3\alpha_{ew})$. Then we obtain $\Gamma_H = 0.2965 \times 10^{-2}$, 1.704×10^{-2} and 0.6511 GeV for $m_H = 120, 150$ and 180 GeV , respectively.

The verification of the independence of the total QCD NLO correction to the $pp \rightarrow W^+W^-b + X$ process on the two cutoffs, δ_s and δ_c , is made. It shows that the total QCD NLO correction $\Delta\sigma_{NLO}$, which is the summation of the three-body and four-body cross sections, is independent of the two cutoffs within the statistical errors. That independence of the full QCD NLO correction to the $pp \rightarrow W^+W^-b + X$ process on the cutoffs δ_s and δ_c provides an indirect check for the correctness of the calculations. In the further numerical calculations, we fix $\delta_s = 1 \times 10^{-3}$ and $\delta_c = \delta_s/50$.

III..2 Event selection criteria

In this subsection we present the description of the event selection criteria. After applying the jet recombination procedure to the protojet events of the $pp \rightarrow W^+W^-b(\bar{b}) + X$ up to the QCD NLO, we obtain the one-jet events and two-jet events. The one-jet event contains only a $b(\bar{b})$ jet or a merged jet involving at least one $b(\bar{b})$ quark, while the two-jet event contains two isolated hard jets which are $b(\bar{b})$ jet and gluon/light-quark jet, respectively. In the following we present detailed criteria for how to treat the one-jet and two-jet events.

(1) For the one-jet events, we collect the events with the constraints on the jet as $p_{T,j} > 25 \text{ GeV}$ and $|y_j| < 2.5$.

(2) For the two-jet events (i.e., $W^+W^-b(\bar{b})j$ ($j = g, q$ and $q = u, \bar{u}, d, \bar{d}, c, \bar{c}, s, \bar{s}$) production), we treat the hard gluon/light-quark jet (j jet), which is noncollinear to the $b(\bar{b})$ jet, either inclusively or exclusively. The inclusive and exclusive two-jet event selection schemes are declared

as follows:

- (i) In the inclusive two-jet event selection scheme both one- and two-jet events are included, no further restriction is applied on the j jet except for the $b(\bar{b})$ jet. The $b(\bar{b})$ jet should satisfy $p_{T,b(\bar{b})} > 25 \text{ GeV}$ and $|y_{b(\bar{b})}| < 2.5$.
- (ii) In the exclusive two-jet event selection scheme, the one-jet events are accepted while the two-jet events are rejected. Therefore, besides the $W^+W^-b(\bar{b})$ production events, we accept the $W^+W^-b(\bar{b})j$ production events only when the $b(\bar{b})$ jet satisfies $p_{T,b(\bar{b})} > 25 \text{ GeV}$ and $|y_{b(\bar{b})}| < 2.5$, and another gluon/light-quark jet (j jet) passes the constraint of either $p_{T,j} < 25 \text{ GeV}$ or $|y_j| > 2.5$. That means the second j jet is undetectable or there is no second separable jet being observed for the $W + W^-b(\bar{b})j$ production events.

The cross sections for the $pp \rightarrow W^+W^-b\bar{b} + X$, $pp \rightarrow W^+W^-bb + X$ and $pp \rightarrow W^+W^-\bar{b}\bar{b} + X$ processes combined with the corresponding additional contributions of the PDFs and the FFs shown in Eqs.(2.14)and (2.15), are free of the quasicollinear mass singularity induced by the $\alpha_s \ln(\mu_{f,r}^2/m_b^2)$ term. Part of these contributions are regarded as the QCD NLO corrections to the $pp \rightarrow W^+W^-b(\bar{b}) + X$ process in the QCD NLO contribution collection scheme-II, where the two $b(\bar{b})$ protojets are merged as one jet. In Table 2, we present the numerical results of the integrated cross sections for the $pp \rightarrow W^+W^-b\bar{b} + X$, $W^+W^-bb + X$, $W^+W^-\bar{b}\bar{b} + X$ processes over three different regions of final state phase space with $m_H = 120, 150$ and 180 GeV , respectively.

III..3 Dependence on energy scale

In Fig.3 we present the integrated LO and the QCD NLO corrected cross sections for the $pp \rightarrow W^+W^-b(\bar{b})+X$ processes at the LHC, as the functions of the renormalization/factorization scale. The full curve is for the LO cross section. The dashed and dotted curves are for the QCD NLO corrected cross sections by taking the QCD NLO contribution collection scheme-I, and adopting the inclusive and exclusive two-jet event selection schemes, separately. The dash-dot-dotted and dash-dotted curves are for the results by taking the QCD NLO contribution collection scheme-II, and adopting the inclusive and exclusive two-jet event selection schemes, respectively.

We can see from Fig.3 that the curve for the LO cross section is relatively smooth, while the QCD NLO corrections in the QCD NLO contribution collection scheme-I make the uncertainty on μ rather large. The QCD NLO corrections in the QCD NLO contribution collection scheme-I by using the inclusive ("exclusive") two-jet event selection scheme change the LO cross section by a factor of between 1.30 (0.51) and 1.99 (1.60) when μ varies from $0.1\mu_0$ to $3\mu_0$. In other words, the scale uncertainties of the QCD NLO corrected cross sections in the QCD NLO contribution collection scheme-I are even worse than that of the LO cross section. This enhancement of the uncertainty of the QCD NLO theoretical predictions is partially due to using the 5FS in calculations, and in this scheme the perturbative series is not ordered strictly by powers of the α_s . Figure 3 shows also that the QCD NLO corrections in the QCD NLO contribution collection scheme-II by adopting the inclusive ("exclusive") two-jet event selection scheme increase the LO cross section by a factor varying from 2.12 (1.59) to 3.54 (2.68) in the plotted range of μ . That shows the QCD corrections in the QCD NLO contribution collection scheme-II violate the convergence of the perturbative series in some ranges of μ , particularly the range of $\mu < 0.5\mu_0$. But we find that the total cross section for the $W^+W^-b(\bar{b})$ production up to the QCD NLO in the QCD NLO contribution collection scheme-II demonstrates a weaker scale uncertainty compared with the LO one. That means the energy scale uncertainty of the LO cross section can be improved by taking the QCD NLO contribution collection scheme-II and adopting either the inclusive or the exclusive two-jet event selection schemes. It just reflects that a stable prediction of the integrated cross section for the $pp \rightarrow W^+W^-b(\bar{b}) + X$ process requires not only a veto on a second isolated hard jet, but also the inclusion of the QCD NLO corrections contributed by the $W^+W^-b\bar{b}(bb, \bar{b}\bar{b})$ production events with the two final $b(\bar{b})$ quarks being merged as one jet. In the further numerical calculations, we take $\mu = \mu_0$ in default of other statements.

III.4 Dependence on Higgs mass

As indicated in the introduction, the $W^+W^-b(\bar{b})$ production may serve as one of the important backgrounds of Higgs-boson production associated with a $b(\bar{b})$ jet, if the Higgs-boson mass is larger than $2m_W$. In this subsection we study the behavior of the QCD NLO corrected cross section for the $pp \rightarrow W^+W^-b + X$ process as a function of the Higgs mass. According to the

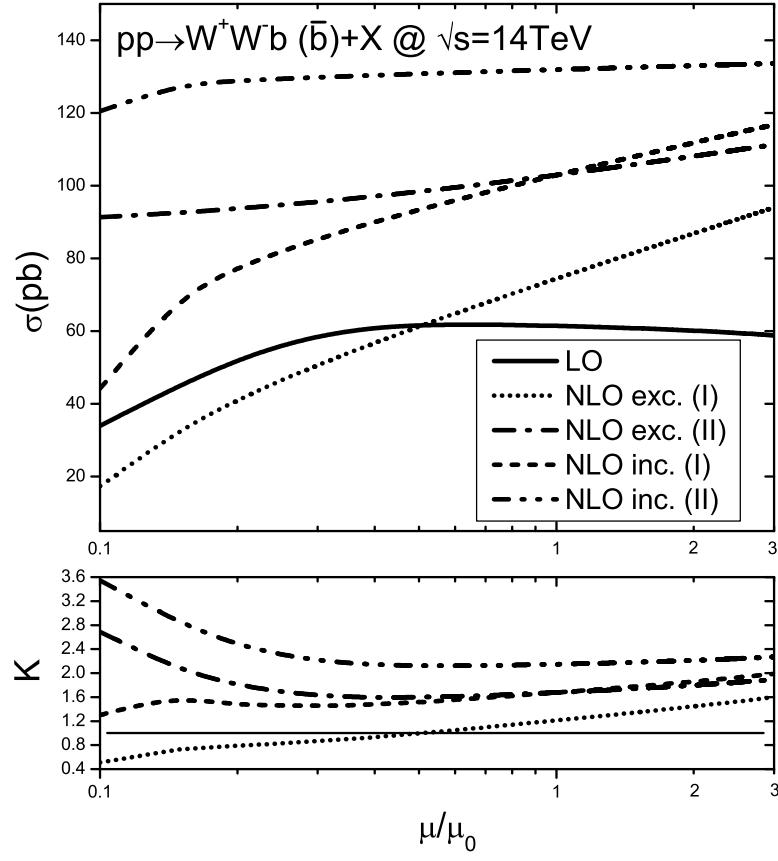


Figure 3: The dependence of the LO and NLO QCD corrected total cross sections for the $pp \rightarrow W^+W^-b + X$ and $pp \rightarrow W^+W^-\bar{b} + X$ processes on μ/μ_0 at the LHC.

| $m_H(\text{GeV})$ | $\sigma_{LO} \text{ (pb)}$ | $\sigma_{NLO} \text{ (inc.) (pb)}$ | K factor | $\sigma_{NLO} \text{ (exc.) (pb)}$ | K factor |
|-------------------|----------------------------|------------------------------------|----------|------------------------------------|----------|
| 120 | 61.86(2) | 102.84(4) | 1.66 | 74.56(2) | 1.21 |
| 150 | 61.84(2) | 102.82(4) | 1.66 | 74.56(2) | 1.21 |
| 180 | 61.96(2) | 102.58(4) | 1.67 | 75.18(2) | 1.21 |

Table 1: The integrated LO and QCD NLO corrected cross sections and the corresponding K factors for the $pp \rightarrow W^+W^-b + X$ and $pp \rightarrow W^+W^-\bar{b} + X$ processes at the LHC by taking the QCD NLO contribution collection scheme-I.

recent Fermilab report[27], the SM Higgs-boson mass has been narrowed down to $114 \sim 158 \text{ GeV}$ and $175 \sim 185 \text{ GeV}$. In our numerical calculations we choose Higgs mass values and their corresponding widths being $\Gamma_H(m_H = 120 \text{ GeV}) = 0.2965 \times 10^{-2} \text{ GeV}$, $\Gamma_H(m_H = 150 \text{ GeV}) = 1.704 \times 10^{-2} \text{ GeV}$ and $\Gamma_H(m_H = 180 \text{ GeV}) = 0.6511 \text{ GeV}$ separately, as provided in Sec.III.1. In Table 1 we present the numerical results of the LO and QCD NLO corrected cross sections, and the corresponding K factors by taking the QCD NLO contribution collection scheme-I with the Higgs-boson mass being 120, 150 and 180 GeV , respectively. The notations of (inc.) and (exc.) refer to the results by adopting the inclusive and exclusive two-jet event selection schemes, separately. From this table we find that the LO and QCD NLO corrected cross sections with both the two two-jet event selection schemes are insensitive to the Higgs-boson mass when m_H varies from 120 to 180 GeV . That is because the contributions of the Feynman diagrams, which correspond to the H^0b production with H^0 subsequently decaying into W pair, are very small.

III.5 $p_{T,b}$ and p_{T,W^\pm} distributions

The LO and QCD NLO corrected distributions of the transverse momentum of the b jet ($p_{T,b}$) and the corresponding K-factors for the $pp \rightarrow W^+W^-b + X$ process at the LHC by taking the QCD NLO contribution collection scheme-I, are demonstrated in Fig.4. The full, dashed and dotted curves are for the LO, QCD NLO corrected $p_{T,b}$ distributions by adopting the inclusive and exclusive two-jet event selection schemes, separately. The corresponding K factors are drawn in the attached figure below. These two figures show that the NLO QCD corrections with both the inclusive and exclusive two-jet event selection schemes always enhance the LO differential cross section $d\sigma_{LO}/dp_{T,b}$, and the NLO QCD corrections to the LO differential cross section

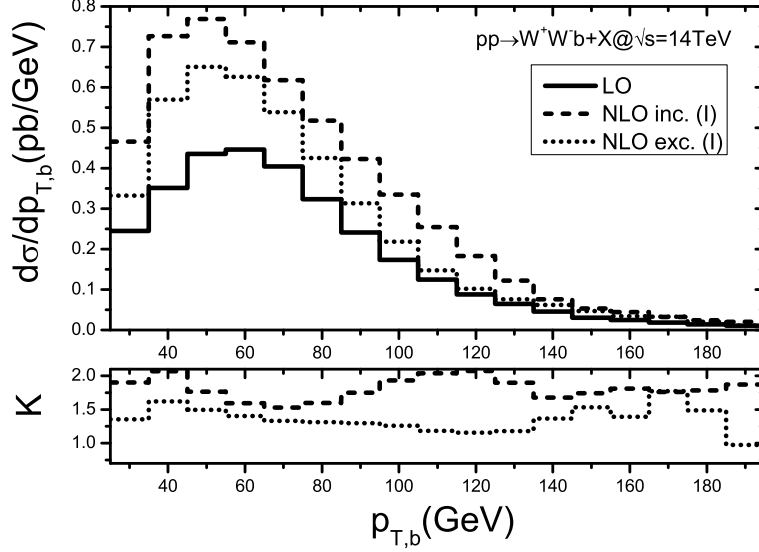


Figure 4: The LO, QCD NLO corrected distributions of the transverse momentum of the bottom jet ($p_{T,b}$) and corresponding K factors for the $pp \rightarrow W^+W^-b + X$ process at the LHC by taking $\mu = \mu_0$, $m_H = 120 \text{ GeV}$ and adopting the QCD NLO contribution collection scheme-I. The corresponding K factors are shown in the figure below.

with the inclusive scheme are always larger than that with the exclusive scheme.

We plot the LO and the QCD NLO corrected distributions of the transverse momenta of W^\pm bosons p_{T,W^+} and p_{T,W^-} for the $pp \rightarrow W^+W^-b + X$ process at the LHC by taking the QCD NLO contribution collection scheme-I in Fig.5(a) and Fig.5(b), respectively. We use the full, dashed and dotted curves describing the LO, QCD NLO corrected distributions with the inclusive and exclusive two-jet event selection schemes, separately. We can see from the figures that the QCD NLO corrections with both the inclusive and exclusive two-jet event selection schemes, always increase the LO differential cross sections $d\sigma_{LO}/dp_{T,W^+}$ and $d\sigma_{LO}/dp_{T,W^-}$, and the enhancement due to the QCD NLO corrections to $d\sigma_{LO}/dp_{T,W}$ with the inclusive two-jet event selection scheme is larger than that with the exclusive two-jet event selection scheme. From the figures we see also that the distributions of the transverse momenta of W^+ and W^- bosons are different.

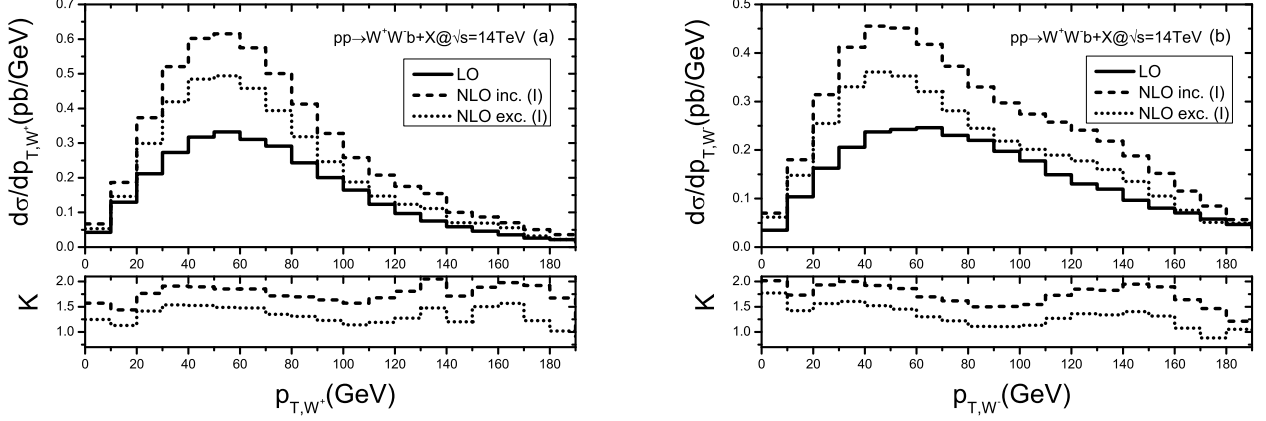


Figure 5: (a) The LO, QCD NLO corrected distributions of the transverse momentum of W^+ boson and the corresponding K factors for the $pp \rightarrow W^+W^-b + X$ process at the LHC. (b) The LO, NLO QCD corrected distributions of the transverse momentum of W^- boson and the corresponding K factors. In these two figures we take $\mu = \mu_0$, $m_H = 120 \text{ GeV}$ and adopt the QCD NLO contribution collection scheme-I.

III..6 Invariant mass $m_{(W+b)}$ distribution

We plot the distributions of the invariant mass of the (W^+b) pair, $m_{(W+b)}$, at the LO and the QCD NLO in Fig.6 with $\mu = \mu_0$ and $m_H = 120 \text{ GeV}$, where the NLO distributions of $m_{(W+b)}$ are presented by taking the QCD NLO contribution collection scheme-I and adopting the inclusive and exclusive two-jet event selection schemes separately. We can see from the figure that the LO and QCD NLO corrected differential cross sections, $d\sigma_{LO}/dm_{(W+b)}$ and $d\sigma_{NLO}/dm_{(W+b)}$, have peaks in the vicinity of $m_{(W+b)} = m_t$. It demonstrates that there is a large contribution part for the process $pp \rightarrow W^+W^-b + X$, which comes from the single top production associated with a W^- boson ($pp \rightarrow bg \rightarrow W^-t$) followed by the subsequential decay of the top quark to W^+b . That is to say the main contribution to the $pp \rightarrow W^+W^-b + X$ process originates from the Feynman diagrams of Figs.1(4,6) at the LO, and their related one-loop diagrams at the NLO. Here we can see that in the invariant mass range around $m_{(W+b)} \sim 171 \text{ GeV}$ the QCD NLO corrections with both the inclusive and exclusive two-jet event selection schemes strongly enhance the LO invariant mass distribution $d\sigma_{LO}/dm_{(W+b)}$, and the QCD NLO correction with the inclusive scheme enhances the LO distribution more heavily than that with the exclusive

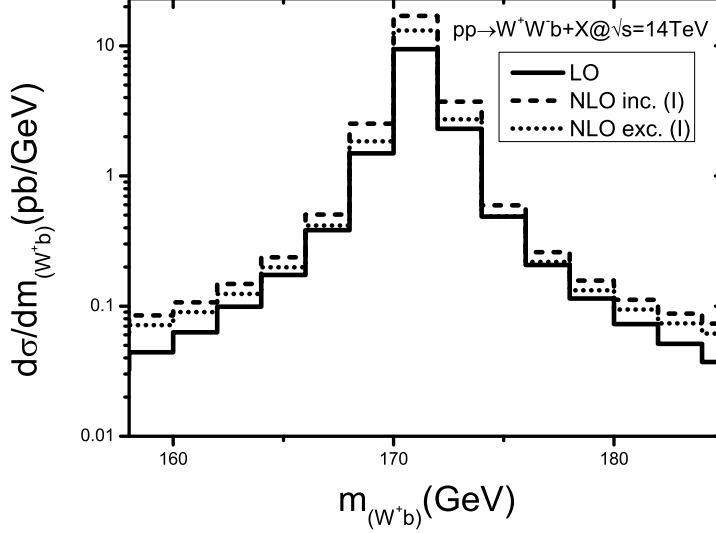


Figure 6: The distributions of the invariant mass of the bottom jet and W^+ boson, $m_{(W^+b)}$, for the $pp \rightarrow W^+W^-b + X$ process at the LHC, where we take $\mu = \mu_0$, $m_H = 120 \text{ GeV}$ and adopt the QCD NLO contribution collection scheme-I.

scheme, particularly around the resonance peak.

III..7 Cross sections for the $pp \rightarrow W^+W^-b\bar{b}$, W^+W^-bb , $W^+W^-b\bar{b}$ processes

In Table 2 we list the numerical results of the integrated cross sections for the three processes $pp \rightarrow W^+W^-b\bar{b}$ and $pp \rightarrow W^+W^-bb$, $b\bar{b}$ with different Higgs-boson mass values. These three $W^+W^-b\bar{b}$, W^+W^-bb and $W^+W^-b\bar{b}$ production processes are induced by the $gg(q\bar{q}) \rightarrow W^+W^-b\bar{b}$, $bb \rightarrow W^+W^-bb$ and $b\bar{b} \rightarrow W^+W^-b\bar{b}$ partonic processes separately. The data in columns (I), (II) and (III) are the integrated cross sections over three different phase-space regions, respectively.

In phase-space region (I), the two $b(\bar{b})$ jets are isolated (i.e., the two $b(\bar{b})$ jets satisfy $\sqrt{\Delta\eta^2 + \Delta\phi^2} > 0.7$), and one $b(\bar{b})$ jet is detectable satisfying the constraints of $p_{T,b(\bar{b})} > 25 \text{ GeV}$ and $|y_{b(\bar{b})}| < 2.5$ while the other $b(\bar{b})$ jet is undetectable, i.e., satisfying $p_{T,b(\bar{b})} < 25 \text{ GeV}$ or $|y_{b(\bar{b})}| > 2.5$.

In phase-space region (II), the two $b(\bar{b})$ jets are merged as one jet (i.e., $\sqrt{\Delta\eta^2 + \Delta\phi^2} < 0.7$), and the merged jet passes the constraints of $p_{T,j} > 25 \text{ GeV}$ and $|y_j| < 2.5$. That is just the

| $m_H(\text{GeV})$ | $WWbb(bb, \bar{b}\bar{b})(\text{I})(\text{pb})$ | $WWbb(bb, \bar{b}\bar{b})(\text{II})(\text{pb})$ | $WWbb(bb, \bar{b}\bar{b})(\text{III})(\text{pb})$ |
|-------------------|---|--|---|
| 120 | 141.66(6) | 27.15(2) | 603.2(1) |
| 150 | 141.54(6) | 27.15(2) | 603.5(1) |
| 180 | 141.28(6) | 27.15(2) | 603.3(1) |

Table 2: The integrated cross sections for the three processes $pp \rightarrow W^+W^-b\bar{b}$, W^+W^-bb , $W^+W^-b\bar{b}$ over three different phase-space regions (I), (II) and (III) with $\mu = \mu_0$, $m_H = 120, 150$ and 180 GeV , respectively.

additional QCD NLO contribution when the QCD NLO contribution collection scheme-II is adopted.

In phase-space region (III), the two $b(\bar{b})$ jets are separately detectable. This means that $\sqrt{\Delta\eta^2 + \Delta\phi^2} > 0.7$ and the two $b(\bar{b})$ jets separately satisfy the constraints of $p_{T,b(\bar{b})} > 25 \text{ GeV}$ and $|y_{b(\bar{b})}| < 2.5$.

Analogy of the data in Table 1, Table 2 shows that the integrated cross sections for the processes $pp \rightarrow W^+W^-b\bar{b}(bb, \bar{b}\bar{b})$ over phase-space regions (I), (II) and (III) are insensitive to the Higgs-boson mass. That means the contributions from the Feynman diagrams, which correspond to the H^0b production followed by the decay of $H^0 \rightarrow W^+W^-$, are rather small. We also find from Table 2 that the integrated cross sections for the $pp \rightarrow W^+W^-b\bar{b}$, $pp \rightarrow W^+W^-bb$ and $pp \rightarrow W^+W^-b\bar{b}$ processes over the three phase-space regions are all rather large, particularly phase-space region (III). Our calculation demonstrates that the contribution from the $pp \rightarrow W^+W^-b\bar{b} + X$ process is the largest one, which has a 2 \sim 3 order larger contribution to the cross section than the other two processes. The large enhancement of this process with the final $b\bar{b}$ pair is due to the large gluon luminosity in PDF at the LHC and the overcompensation of the top quark resonances in the $pp \rightarrow t\bar{t} \rightarrow W^+W^-b\bar{b} + X$ process.

IV. Summary

In this paper we calculate the full QCD NLO corrections to the W -pair production in association with a massive (anti)bottom jet in the SM at the LHC, which is an important background of the single top production and can be used to search for new physics beyond the SM by using the five-flavor scheme. The dependence of the integrated cross sections on the factoriza-

tion/renormalization scale and the Higgs mass is studied. We also investigate the QCD NLO corrections to the distributions of the transverse momenta ($\frac{d\sigma}{dp_T}$) of the final particles. Our numerical results show that by taking the QCD NLO contribution collection scheme-I and adopting the inclusive (exclusive) two-jet event selection scheme, the K factor of the total cross section for the $pp \rightarrow W^+W^-b(\bar{b}) + X$ process at the LHC can reach 1.66 (1.21) with $\mu = \mu_0$. We find that the LO integrated and differential cross sections are modified by the QCD NLO radiative corrections obviously, and the QCD NLO corrections to the $W^+W^-b(\bar{b})$ production process with the QCD NLO contribution collection scheme-I can not reduce the scale uncertainty of the LO cross section for the $pp \rightarrow W^+W^-b(\bar{b}) + X$ process at the LHC by adopting either the inclusive or exclusive two-jet event selection schemes. The stable prediction for the integrated cross section requires not only a veto on a second isolated hard jet, but also the inclusion of the QCD NLO correction contributed by the $W^+W^-b\bar{b}(bb, \bar{b}\bar{b})$ production events with the two final $b(\bar{b})$ quarks being merged as one jet.

Acknowledgments: This work was supported in part by the National Natural Science Foundation of China (Contract No.10875112, No.11075150, No.11005101), and the Specialized Research Fund for the Doctoral Program of Higher Education (Contract No.20093402110030).

References

- [1] T. M. P. Tait, Phys. Rev. **D 61**, 034001(1999); J. Alwall et al., Eur. Phys. J. C. **49**, 791 (2007); J. A. Aguilar-Saavedra and A. Onofre, Phys. Rev. **D 83**, 073003 (2011).
- [2] Tevatron Electroweak Working Group for CDF and D0, [arXiv:0908.2171].
- [3] D0 Collaboration, Phys. Rev. Lett. 103 (2009) 092001 , [arXiv:0903.0850]; D0 Collaboration, Phys.Lett.**B682** (2010) 363 ,[arXiv:0907.4259]; CDF Collaboration,Phys.Rev.Lett.103 (2009) 092002 , [arXiv:0903.0885].
- [4] Carlson D. O. and Yuan C. P., Phys. Lett. **B306** (1993) 386; Mahlon G. and Parke S. J., Phys. Rev. **D55** (1997) 7249, [arXiv:hep-ph/9611367]; Heinson A. P., Belyaev A. S. and

- Boos E. E., Phys. Rev. **D56** (1997) 3114, [arXiv:hep-ph/9612424]; Mahlon G. and Parke S. J., Phys. Lett. **B476** (2000) 323, [arXiv:hep-ph/9912458]; Sullivan Z., Phys. Rev. **D72** (2005) 094034, [arXiv:hep-ph/0510224].
- [5] C. E. Gerber et al., Report No. FERMILAB-CONF-07-052, (2007), and references therein (unpublished).
- [6] B. Mellado, W. Quayle, Sau Lan Wu, TeV4LHC workshop, 29 April 2005; B. Mellado, W. Quayle and S. L. Wu, Phys. Rev. **D76**, 093007 (2007), [arXiv:0708.2507].
- [7] Stefan Dittmaier, Stefan Kallweit, and Peter Uwer, Nucl. Phys. **B826** (2010) 18-70, [arXiv:0908.4124]; 'NLO QCD corrections to WW+jet production including leptonic W decays at hadron colliders', FR-PHENO-2010-002, PSI-PR-10-04, HU-EP-10/02, [arxiv 1001.2427].
- [8] John M. Campbell, R. Keith Ellis, Giulia Zanderighi, JHEP 0712 (2007) 056, [arXiv:0710.1832].
- [9] T. Hahn, Comput. Phys. Commun. **140** (2001) 418.
- [10] T. Hahn, M. Perez-Victoria, Comput. Phys. Commun. **118** (1999) 153.
- [11] A. Denner, S. Dittmaier, M. Roth, D. Wackeroth, Nucl. Phys. **B560** (1999) 33; A. Denner, S. Dittmaier, M. Roth, L.H. Wieders, Nucl. Phys. **B724** (2005) 247.
- [12] S.D. Ellis and D.E. Soper, Phys. Rev. **D48** (1993) 3160, [arXiv:hep-ph/9305266].
- [13] B. W. Harris and J. F. Owens, Phys. Rev. **D65** (2002) 094032, [arxiv:hep-ph/0102128].
- [14] J. Collins, F. Wilczek, and A. Zee, Phys. Rev. **D 18**, 242 (1978); W. J. Marciano, Phys. Rev. **D 29**, 580 (1984); P. Nason, S. Dawson, R.K. Ellis, Nucl. Phys. **B 327**, 49 (1989); Nucl. Phys. **B 335**, 260(E) (1989).
- [15] R. K. Ellis, G. Zanderighi, JHEP 0802 (2008) 002, [arXiv:0712.1851].
- [16] G.'t Hooft and M. Veltman, Nucl. Phys. **B153** (1979) 365.

- [17] A. Denner, U. Nierste and R. Scharf, Nucl. Phys. **B367** (1991) 637.
- [18] A. Denner and S. Dittmaier, Nucl. Phys. **B658** (2003) 175.
- [19] G. J. van Oldenborgh, Comput. Phys. Commun. **66**, 1 (1991).
- [20] G. P. Lepage, J. Comput. Phys. 27 (1978) 192 and CLNS-80/447.
- [21] J. Collins Phys.Rev. **D58** (1998) 094002.
- [22] B. A. Kniehl, G. Krämer, I. Schienbein, and H. Spiesberger, Eur. Phys. J. **C 41**, 199 (2005);
S. Kretzer and I. Schienbein, Phys. Rev. **D 58**, 094035 (1998); M. Krämer, F. Olness, and
D. Soper, Phys. Rev. **D 62**, 096007 (2000); F. Olness, R. Scalise and W-K. Tung, Phys.
Rev. **D 59**, 014506 (1998).
- [23] C. Amsler, *et al.* Phys. Lett. **B667** (2008) 1 .
- [24] J. Pumplin *et al.*, JHEP 0207 (2002) 012 ; D. Stump *et al.*, JHEP 0310 (2003) 046 .
- [25] M. Jezabek and J.H. Kühn, Nucl. Phys. **B314** (1989) 1.
- [26] A. Djouadi, J. Kalinowski, M. Spira, Comput. Phys. Commun. 108 (1998) 56.
- [27] The CDF Collaboration, the D0 Collaboration, the Tevatron New Physics, and
Higgs Working Group, Fermilab, Report No. FERMILAB-CONF-10-257-E, (2010),
[arXiv:1007.4587v1].